

Article

Bulk Viscosity of Relativistic $npe\mu$ Matter in Neutron-Star Mergers

Mark Alford ¹ , Arus Harutyunyan ^{2,3,*}  and Armen Sedrakian ^{4,5} 

- ¹ Department of Physics, Washington University, St. Louis, MO 63130, USA
² Byurakan Astrophysical Observatory, National Academy of Sciences, Byurakan 0213, Armenia
³ Department of Physics, Yerevan State University, Yerevan 0025, Armenia
⁴ Frankfurt Institute for Advanced Studies, D-60438 Frankfurt am Main, Germany
⁵ Institute of Theoretical Physics, University of Wrocław, 50-204 Wrocław, Poland
* Correspondence: arus@bao.sci.am

Abstract: We discuss the bulk viscosity of hot and dense $npe\mu$ matter arising from weak-interaction direct Urca processes. We consider two regimes of interest: (a) the neutrino-transparent regime with $T \leq T_{\text{tr}}$ ($T_{\text{tr}} \simeq 5 \div 10$ MeV is the neutrino-trapping temperature); and (b) the neutrino-trapped regime with $T \geq T_{\text{tr}}$. Nuclear matter is modeled in relativistic density functional approach with density-dependent parametrization DDME2. The maximum of the bulk viscosity is achieved at temperatures $T \simeq 5 \div 6$ MeV in the neutrino-transparent regime, then it drops rapidly at higher temperatures where neutrino-trapping occurs. As an astrophysical application, we estimate the damping timescales of density oscillations by the bulk viscosity in neutron star mergers and find that, e.g., at the oscillation frequency $f = 10$ kHz, the damping will be very efficient at temperatures $4 \leq T \leq 7$ MeV where the bulk viscosity might affect the evolution of the post-merger object.

Keywords: bulk viscosity; weak processes; $npe\mu$ matter; binary neutron star mergers; damping of density oscillations

1. Introduction

The recent detections of gravitational waves from binary neutron-star (BNS) mergers by the LIGO-Virgo collaboration motivate studies of the transport properties of hot and dense nuclear matter. Numerical simulations of BNS mergers predict intense emission of gravitational waves during the first tens of milliseconds after the merger in the kHz frequency range (see, e.g., Refs. [1–4] for recent simulations). The dissipation of matter flows in the post-merger object might affect the gravitational wave spectra emitted during this stage of BNS merger evolution. In particular, indications of bulk viscous dissipation were seen in a recent BNS simulation incorporating beta equilibrating processes [5], confirming earlier estimates of its likely importance.

There exist extensive studies of the bulk viscosity of neutron–proton–electron (hereafter npe) and $npe\mu$ (where μ stands for muons) matters in low-temperature (cold) neutron stars [6–16]. The bulk viscosity of the dense matter at high temperatures (up to tens of MeV) was computed in recent works which covered various regimes of temperature and density, as well as neutrino trapping/un-trapping, in strongly interacting hadronic matter [17–20].

In this contribution, we review briefly the results of Ref. [20] for the bulk viscosity of the neutrino-trapped, relativistic $npe\mu$ matter, as well as complement them with novel results for the neutrino-transparent regime. The impact of purely leptonic weak processes on the bulk viscosity is discussed. We use the DDME2 parametrization [21] of relativistic density functional

arXiv:2209.04717v1 [astro-ph.HE] 10 Sep 2022



Citation: Alford, M.; Harutyunyan, A.; Sedrakian, A. Bulk Viscosity of Relativistic $npe\mu$ Matter in Neutron-Star Mergers. *Particles* **2022**, *5*, 361–378. <https://doi.org/10.3390/particles5030029>

Academic Editor: Nicolas Chamel

Received: 30 July 2022

Accepted: 31 August 2022

Published: 6 September 2022

Publisher's Note: MDPI stays neutral with regard to jurisdictional claims in published maps and institutional affiliations.



Copyright: © 2022 by the authors. Licensee MDPI, Basel, Switzerland. This article is an open access article distributed under the terms and conditions of the Creative Commons Attribution (CC BY) license (<https://creativecommons.org/licenses/by/4.0/>).

theory with density-dependent couplings to model the background nuclear matter. It provides very reasonable values of such characteristics of symmetric nuclear matter, as the energy per nucleon $E_{\text{sat}} = -16.14$ MeV and compressibility $K_{\text{sat}} = 251.15$ MeV at saturation density $n_0 = 0.152 \text{ fm}^{-3}$, as well as characteristics of asymmetric nuclear matter such as the symmetry energy $E_{\text{sym}} = 32.31$ MeV and its slope $L_{\text{sym}} = 51.27$ MeV. In our previous work [18,20] we used the NL3 parameterization (along with the DDME2) where the couplings are density-independent but meson fields acquire additional self-interactions terms. This functional differs significantly from the DDME2 functional used in this study in the properties of asymmetric matter with $E_{\text{sym}} = 37.4$ and $L_{\text{sym}} = 118.9$ MeV. Specifically, these two functionals cover well the range for the parameters E_{sym} and L_{sym} that have been inferred from the PREX-II experiment by two alternative analysis [22,23]. Thus, using our previous results one can assess the impact of the variations of the important characteristics of nuclear matter on the various quantities of interest, such as bulk viscosity and damping time scales. A full analysis of the sensitivity of the results on the input of various density functionals goes beyond the present study.

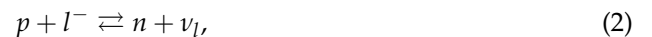
With the results obtained for the bulk viscosity, we estimate the bulk viscous dissipation timescales of density oscillations in BNS mergers. For typical oscillation frequencies $1 \leq f \leq 10$ kHz the bulk viscous damping timescales reach down to tens of milliseconds (at $n_B \simeq 3n_0$) or milliseconds (at $n_B \simeq n_0$) at temperatures $4 \leq T \leq 7$ MeV. Here the bulk viscous damping can have a significant impact on the initial phase of post-merger dynamics with a typical timescale ~ 10 ms. At high temperatures above the neutrino-trapping, the bulk viscosity falls rapidly by orders of magnitude, and the damping timescales become too long to affect the dynamics of BNS mergers.

This paper is organized as follows. In Section 2, we discuss the weak processes in nuclear matter. In Section 3, we discuss the bulk viscosity produced by the Urca processes. Section 4 collects the numerical results for the equilibration rates, the bulk viscosity, and the dissipation damping timescales in the regimes of neutrino-transparent and neutrino-trapped matter. Section 5 provides a brief summary of our results. We work with natural (Gaussian) units where $\hbar = c = k_B = 1$.

2. Weak Processes in Neutron Star Matter

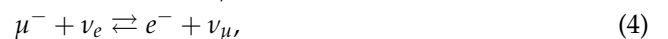
We consider relativistic $npe\mu$ matter in the range of densities $0.5n_0 \leq n_B \leq 5n_0$, where $n_0 \simeq 0.152 \text{ fm}^{-3}$ is the nuclear saturation density and temperatures $1 \leq T \leq 100$ MeV. Neutrinos are trapped in the matter above the neutrino-trapping temperature $T_{\text{tr}} \simeq 5 \div 10$ MeV and un-trapped (free-streaming) below this temperature [24].

Consider now the simplest semi-baryonic β -equilibration processes—the direct Urca processes of neutron decay and lepton capture, respectively



where $l = \{e, \mu\}$ is electron or muon, ν_l is the corresponding neutrino. In the ν -transparent regime, these processes proceed only in one direction from left to right as neutrinos/anti-neutrinos can appear only in the final state.

If muons are present in matter, the following leptonic processes of muon decay, neutrino absorption and antineutrino absorption, respectively, may occur additionally



In the ν -transparent regime, (4) and (5) are not possible, and (3) can only occur in the forward direction when the temperature is high enough to open up enough phase space around the muon and electron Fermi surfaces. We neglect modified-Urca-type processes involving electromagnetic interaction with a spectator particle [15]; these are suppressed by a factor of α^2 .

In $npe\mu$ matter the baryon number given by $n_B = n_n + n_p$ is conserved. The matter is also charge neutral, i.e., $n_p = n_e + n_\mu$. In the neutrino-trapped case the lepton numbers $n_{L_i} = n_l + n_{\nu_l} = Y_{L_i} n_B$ (with Y_{L_i} being the lepton fractions) are also conserved. In neutron star mergers one can adopt the values $Y_{Le} = Y_{L\mu} = 0.1$ for the neutrino-trapped case [25].

The β -equilibration rates of the processes (1) and (2) are given, respectively, by

$$\Gamma_{n \rightarrow pl\bar{\nu}} = \int d\Omega_p \sum |\mathcal{M}_{\text{Urca}}|^2 \bar{f}(k) \bar{f}(p) \bar{f}(k') f(p') (2\pi)^4 \delta^{(4)}(k + p + k' - p'), \quad (6)$$

$$\Gamma_{pl \rightarrow n\nu} = \int d\Omega_p \sum |\mathcal{M}_{\text{Urca}}|^2 f(k) f(p) \bar{f}(k') \bar{f}(p') (2\pi)^4 \delta(k + p - k' - p'). \quad (7)$$

where

$$\int d\Omega_p = \int \frac{d^3p}{(2\pi)^3 2p_0} \int \frac{d^3p'}{(2\pi)^3 2p'_0} \int \frac{d^3k}{(2\pi)^3 2k_0} \int \frac{d^3k'}{(2\pi)^3 2k'_0} \quad (8)$$

is the Lorentz-invariant momentum phase-space element, $f(p)$ is the Fermi distribution of particles, and $\bar{f}(p) = 1 - f(p)$. The particles are assigned momenta as follows: $(l) \rightarrow k$, $(\nu_l/\bar{\nu}_l) \rightarrow k'$, $(p) \rightarrow p$, and $(n) \rightarrow p'$. Note that in neutrino-transparent matter one should replace $\bar{f}(k') \rightarrow 1$ in these expressions.

The spin-averaged relativistic matrix element of the Urca processes reads [26]

$$\begin{aligned} \sum |\mathcal{M}_{\text{Urca}}|^2 = & 32G_F^2 \cos^2 \theta_c \left[(1 + g_A)^2 (k \cdot p)(k' \cdot p') \right. \\ & \left. + (1 - g_A)^2 (k \cdot p')(k' \cdot p) + (g_A^2 - 1)m^{*2}(k \cdot k') \right], \end{aligned} \quad (9)$$

where $G_F = 1.166 \cdot 10^{-5} \text{ GeV}^{-2}$ is the Fermi coupling constant, θ_c is the Cabibbo angle with $\cos \theta_c = 0.974$, $g_A = 1.26$ is the axial-vector coupling constant, and m^* is the effective nucleon mass. We will keep only the first term of this expression in the following as the second and the third terms are negligible for g_A values close to the vacuum value quoted above. The twelve-dimensional phase-space integrals in Equations (6) and (7) can be reduced to the following four-dimensional integrals which are then computed numerically [20]

$$\begin{aligned} \Gamma_{n \rightarrow pl\bar{\nu}}(\mu_{\Delta_l}) = & -\frac{G^2 T^4}{(2\pi)^5} \int_{-\infty}^{\infty} dy \int_0^{\infty} dx \left[(\mu_{\nu_l} + \mu_n^* + yT)^2 - m_n^{*2} - x^2 T^2 \right] \\ & \times \left[(\mu_l + \mu_p^* + \bar{y}_l T)^2 - m_l^2 - m_p^{*2} - x^2 T^2 \right] \\ & \times \int_{m_l/T - \alpha_l}^{\alpha_p + \bar{y}_l} dz \bar{f}(z) f(z - \bar{y}_l) \theta_x \int_{\alpha_{\nu_l}}^{\infty} dz' f(z' + y) \bar{f}(z') \theta_y, \end{aligned} \quad (10)$$

$$\begin{aligned} \Gamma_{pl \rightarrow n\nu}(\mu_{\Delta_l}) = & \frac{G^2 T^4}{(2\pi)^5} \int_{-\infty}^{\infty} dy \int_0^{\infty} dx \left[(\mu_{\nu_l} + \mu_n^* + yT)^2 - m_n^{*2} - x^2 T^2 \right] \\ & \times \left[(\mu_l + \mu_p^* + \bar{y}_l T)^2 - m_l^2 - m_p^{*2} - x^2 T^2 \right] \\ & \times \int_{m_l/T - \alpha_l}^{\alpha_p + \bar{y}_l} dz f(z) f(\bar{y}_l - z) \theta_x \int_{-\alpha_{\nu_l}}^{\alpha_n + y} dz' f(z' - y) \bar{f}(z') \theta_z, \end{aligned} \quad (11)$$

where $G = G_F \cos \theta_c (1 + g_A)$, m_l is the lepton mass, $\alpha_l = \mu_l/T$, $\alpha_N = \mu_N^*/T$ for $N = \{n, p\}$ with μ_N^* being the nucleon effective chemical potential, see Section 4.1. Here $\bar{y}_l = y + \mu_{\Delta_l}/T$ with $\mu_{\Delta_l} = \mu_n + \mu_{\nu_l} - \mu_p - \mu_l$ and $f(x) \equiv [1 + e^x]^{-1}$. The θ -functions in Equations (10) and (11) imply

$$\theta_x : (z_k - x)^2 \leq (z - \alpha_p - \bar{y}_l)^2 - m_p^{*2}/T^2 \leq (z_k + x)^2, \tag{12}$$

$$\theta_y : (z'_k - x)^2 \leq (z' + \alpha_n + y)^2 - m_n^{*2}/T^2 \leq (z'_k + x)^2, \tag{13}$$

$$\theta_z : (z'_k - x)^2 \leq (z' - \alpha_n - y)^2 - m_n^{*2}/T^2 \leq (z'_k + x)^2. \tag{14}$$

The integration variables y and x are the transferred energy and momentum, respectively, normalized by the temperature; the variables z and z' are the normalized-by-temperature lepton and neutrino energies, respectively, computed from their chemical potentials, $z_k = \sqrt{(z + \alpha_l)^2 - m_l^2/T^2}$ and $z'_k = z' \mp \alpha_{\nu_l}$ are the normalized-by-temperature momenta of the lepton and the antineutrino/neutrino, respectively. In the case of neutrino-trapped matter, the rates of the inverse processes are obtained from Equations (10) and (11) by replacing $f(p_i) \rightarrow \bar{f}(p_i)$ for all particles. In the case of ν -transparent matter the inverse processes are not allowed, and one should replace $\mu_{\nu_l} = 0$ and $\bar{f}(z') \rightarrow 1$ in the direct processes.

We will work in the low-temperature approximation where beta equilibrium corresponds to $\mu_{\Delta_l} = 0$. In the case of deviations from β -equilibrium, there is a net rate of proton production/annihilation due to each of the processes (1) and (2), which in the linear-response regime $\mu_{\Delta_l} \ll T$ can be written as $\Gamma_{n \rightarrow pl\bar{\nu}} - \Gamma_{pl\bar{\nu} \rightarrow n} = \lambda_{n \leftrightarrow pl\bar{\nu}} \mu_{\Delta_l}$, and $\Gamma_{n\nu \rightarrow pl} - \Gamma_{pl \rightarrow n\nu} = \lambda_{pl \leftrightarrow n\nu} \mu_{\Delta_l}$, with the coefficients $\lambda_{n \leftrightarrow pl\bar{\nu}}$ and $\lambda_{pl \leftrightarrow n\nu}$ given by [20]

$$\lambda_{n \leftrightarrow pl\bar{\nu}} = \left(\frac{\partial \Gamma_{n \rightarrow pl\bar{\nu}}}{\partial \mu_{\Delta_l}} - \frac{\partial \Gamma_{pl\bar{\nu} \rightarrow n}}{\partial \mu_{\Delta_l}} \right) \Big|_{\mu_{\Delta_l}=0} = \frac{\Gamma_{n \leftrightarrow pl\bar{\nu}}}{T}, \tag{15}$$

$$\lambda_{pl \leftrightarrow n\nu} = \left(\frac{\partial \Gamma_{n\nu \rightarrow pl}}{\partial \mu_{\Delta_l}} - \frac{\partial \Gamma_{pl \rightarrow n\nu}}{\partial \mu_{\Delta_l}} \right) \Big|_{\mu_{\Delta_l}=0} = \frac{\Gamma_{pl \leftrightarrow n\nu}}{T}. \tag{16}$$

Note that at temperatures $T \gtrsim 1$ MeV and at densities where direct Urca would be forbidden at $T = 0$, the neutron decay and lepton capture processes are Boltzmann-suppressed by different factors, arising from their different phase spaces [24]. This means that the coefficients should be evaluated at a nonzero $\mu_{\Delta_l} = \mu_{\Delta_l}^{\text{eq}}$, but we work in the approximation $\mu_{\Delta_l}^{\text{eq}} = 0$: this is discussed in Section 4.

Similar to the Urca reaction rates, the lepton reaction rates can be written in the following form

$$\Gamma_{\mu \rightarrow e\bar{\nu}\nu} = \int d\Omega_k \sum |\mathcal{M}_{\text{lep}}|^2 f(k_\mu) \bar{f}(k_e) \bar{f}(k_{\bar{\nu}_e}) \bar{f}(k_{\nu_\mu}) (2\pi)^4 \delta^{(4)}(k_e + k_{\bar{\nu}_e} + k_{\nu_\mu} - k_\mu), \tag{17}$$

$$\Gamma_{\mu\nu \rightarrow e\nu} = \int d\Omega_k \sum |\mathcal{M}_{\text{lep}}|^2 f(k_\mu) f(k_{\nu_e}) \bar{f}(k_e) \bar{f}(k_{\nu_\mu}) (2\pi)^4 \delta^{(4)}(k_e + k_{\nu_\mu} - k_{\nu_e} - k_\mu), \tag{18}$$

$$\Gamma_{\mu\bar{\nu} \rightarrow e\bar{\nu}} = \int d\Omega_k \sum |\mathcal{M}_{\text{lep}}|^2 f(k_\mu) f(k_{\bar{\nu}_\mu}) \bar{f}(k_e) \bar{f}(k_{\bar{\nu}_e}) (2\pi)^4 \delta^{(4)}(k_e + k_{\bar{\nu}_e} - k_{\bar{\nu}_\mu} - k_\mu), \tag{19}$$

where $d\Omega_k$ is defined analogously to Equation (8). The spin-averaged relativistic matrix element of lepton reactions reads [27]

$$\sum |\mathcal{M}_{\text{lep}}|^2 = 128G_F^2 (k_e \cdot k_{\nu_\mu/\bar{\nu}_\mu}) (k_{\nu_e/\bar{\nu}_e} \cdot k_\mu). \tag{20}$$

The final expressions for the lepton reaction rates are very similar to the Urca process rates (10) and (11) and are given in Ref. [20].

3. Bulk Viscosity of $npe\mu$ Matter

In this section, we briefly review the bulk viscosity of relativistic $npe\mu$ matter arising from the Urca processes (1) and (2). For this, we consider small-amplitude density oscillations with frequency ω . Separating the oscillating parts from the static equilibrium values of particle densities we can write $n_j(t) = n_{j0} + \delta n_j(t)$, where $\delta n_j(t) \sim e^{i\omega t}$ with $j = \{n, p, l, \nu_l\}$. Oscillations drive the system out of chemical equilibrium leading to nonzero chemical imbalances $\mu_{\Delta_l} = \delta\mu_n + \delta\mu_{\nu_l} - \delta\mu_p - \delta\mu_l$, which can be written as

$$\mu_{\Delta_l} = A_n\delta n_n + A_{\nu_e}\delta n_{\nu_e} - A_p\delta n_p - A_l\delta n_l, \tag{21}$$

where the particle susceptibilities are defined as $A_n = A_{nn} - A_{pn}$, $A_p = A_{pp} - A_{np}$, and $A_l = A_{ll}$, $A_{\nu_l} = A_{\nu_l\nu_l}$ with

$$A_{ij} = \frac{\partial\mu_i}{\partial n_j}, \tag{22}$$

where the derivatives are computed in β -equilibrium state.

If the weak processes were switched off, then the number of all particle species would conserve separately, which implies

$$\frac{\partial}{\partial t}\delta n_j^0(t) + \theta n_{j0} = 0 \quad \Rightarrow \quad \delta n_j^0(t) = -\frac{\theta}{i\omega} n_{j0}, \tag{23}$$

where $\theta = \partial_i v^i$ is the fluid expansion rate. Once the weak reactions are switched on, there is a net production of particles which should be included in the balance equations. To linear order in chemical imbalances, these equations read

$$\frac{\partial}{\partial t}\delta n_n(t) + \theta n_{n0} = -\lambda_e\mu_{\Delta_e}(t) - \lambda_\mu\mu_{\Delta_\mu}(t), \tag{24}$$

$$\frac{\partial}{\partial t}\delta n_p(t) + \theta n_{p0} = \lambda_e\mu_{\Delta_e}(t) + \lambda_\mu\mu_{\Delta_\mu}(t), \tag{25}$$

$$\frac{\partial}{\partial t}\delta n_e(t) + \theta n_{e0} = \lambda_e\mu_{\Delta_e}(t) + \lambda_L\mu_{\Delta}^L(t), \tag{26}$$

$$\frac{\partial}{\partial t}\delta n_\mu(t) + \theta n_{\mu0} = \lambda_\mu\mu_{\Delta_\mu}(t) - \lambda_L\mu_{\Delta}^L(t), \tag{27}$$

where $\mu_{\Delta}^L \equiv \mu_\mu + \mu_{\nu_e} - \mu_e - \mu_{\nu_\mu} = \mu_{\Delta_e} - \mu_{\Delta_\mu}$ is the chemical imbalance for leptons, and $\lambda_l = \lambda_{n\leftrightarrow pl\bar{\nu}} + \lambda_{pl\leftrightarrow n\nu}$. The coefficient λ_L is the purely leptonic analog to λ_l .

Solving the system of Equations (24)–(27) is generally quite cumbersome. However, as shown in Section 4.1, the lepton processes proceed typically much slower than the Urca processes in both regimes of neutrino-transparent and neutrino-trapped matter, i.e., $\lambda_L \ll \lambda_l$ (slow lepton-equilibration limit). As a result, the terms $\propto \lambda_L$ can be dropped from the balance Equations (24)–(27). In other words, the Urca-process-driven bulk viscosity can be computed by assuming that the weak leptonic processes are frozen.

Substituting now Equation (21) in Equations (24) and (26) and putting $\lambda_L = 0$ we find

$$i\omega\delta n_n = -n_{n0}\theta - (\lambda_e + \lambda_\mu)A_n\delta n_n + (\lambda_e + \lambda_\mu)A_p\delta n_p + \lambda_e A_e\delta n_e + \lambda_\mu A_\mu\delta n_\mu - \lambda_e A_{\nu_e}\delta n_{\nu_e} - \lambda_\mu A_{\nu_\mu}\delta n_{\nu_\mu}, \tag{28}$$

$$i\omega\delta n_e = -n_{e0}\theta + \lambda_e A_n\delta n_n - \lambda_e A_p\delta n_p - \lambda_e A_e\delta n_e + \lambda_e A_{\nu_e}\delta n_{\nu_e}. \tag{29}$$

Using the relations $\delta n_p + \delta n_n = \delta n_B$, $\delta n_e + \delta n_\mu = \delta n_p$, $\delta n_{L_e} = \delta n_e + \delta n_{\nu_e}$, and $\delta n_{L_\mu} = \delta n_\mu + \delta n_{\nu_\mu}$ and solving the coupled Equations (28) and (29) we find ($\lambda \equiv \lambda_e + \lambda_\mu$)

$$\begin{aligned}
 D\delta n_n &= -\frac{\theta}{i\omega} \left\{ i\omega \left[n_{n0}(i\omega + \lambda_e A_e + \lambda_e A_{\nu_e}) + n_{e0}(\lambda_e A_e + \lambda_e A_{\nu_e} - \lambda_\mu A_\mu - \lambda_\mu A_{\nu_\mu}) \right] \right. \\
 &+ \left[i\omega(\lambda A_p + \lambda_\mu A_\mu + \lambda_\mu A_{\nu_\mu}) + \lambda_e \lambda_\mu ((A_1 - A_n)(A_2 - A_n) - A_p^2) \right] n_{B0} \\
 &\left. - \lambda_e A_{\nu_e} \left[i\omega + \lambda_\mu (A_\mu + A_{\nu_\mu}) \right] n_{L_e0} - \lambda_\mu A_{\nu_\mu} \left[i\omega + \lambda_e (A_e + A_{\nu_e}) \right] n_{L_\mu0} \right\}, \tag{30}
 \end{aligned}$$

$$\begin{aligned}
 D\delta n_e &= -\frac{\theta}{i\omega} \left\{ i\omega n_{e0} \left[i\omega + \lambda_\mu A_2 + \lambda_e (A_n + A_p) \right] \right. \\
 &- \lambda_e n_{B0} \left[A_p(i\omega + \lambda_\mu A_2) - \lambda_\mu (A_n + A_p)(A_2 - A_n) \right] \\
 &+ \lambda_e n_{L_e0} A_{\nu_e} (i\omega + \lambda_\mu A_2) + \lambda_e (A_n + A_p) i\omega n_{n0} \\
 &\left. - \lambda_e \lambda_\mu (A_n + A_p) A_{\nu_\mu} n_{L_\mu0} \right\}, \tag{31}
 \end{aligned}$$

where we used the baryon and lepton number conservation $\delta n_B = -n_{B0}(\theta/i\omega)$ and $\delta n_{L_l} = -n_{L_l0}(\theta/i\omega)$, and defined

$$D = (i\omega + \lambda_e A_1)(i\omega + \lambda_\mu A_2) - \lambda_e \lambda_\mu (A_n + A_p)^2 \tag{32}$$

with

$$A_1 = A_n + A_p + A_e + A_{\nu_e}, \tag{33}$$

$$A_2 = A_n + A_p + A_\mu + A_{\nu_\mu}. \tag{34}$$

In order to find the bulk viscosity we still need to separate the instantaneous equilibrium parts of particle densities from perturbations (30) and (31). Equilibrium shifts can be obtained from Equations (30) and (31) either in the limit of $\lambda_l \rightarrow \infty$ (fast equilibration), or in the limit of $\lambda_l \rightarrow 0$ (slow equilibration). Both choices lead us to the same result for the bulk viscosity as the latter vanishes in both limits of fast or slow equilibration. Subtracting thus the local quasi-equilibrium shifts δn_j^0 from Equations (30) and (31) we find the required nonequilibrium parts $\delta n'_j = \delta n_j - \delta n_j^0$. After this the nonequilibrium part of the pressure, referred to as bulk viscous pressure, will be given by

$$\Pi = \sum_j c_j \delta n'_j, \tag{35}$$

with

$$c_j \equiv \frac{\partial p}{\partial n_j} = \sum_i n_{i0} \frac{\partial \mu_i}{\partial n_j} = \sum_i n_{i0} A_{ij}. \tag{36}$$

Here we used the Gibbs–Duhem relation $dp = sdT + \sum_i n_i d\mu_i$, and recalled the definitions (22). The bulk viscous pressure then reads

$$\Pi = \frac{\theta}{i\omega} \frac{i\omega(\lambda_e C_1^2 + \lambda_\mu C_2^2) + \lambda_e \lambda_\mu [A_1 C_2^2 + A_2 C_1^2 - 2(A_n + A_p)C_1 C_2]}{(i\omega + \lambda_e A_1)(i\omega + \lambda_\mu A_2) - \lambda_e \lambda_\mu (A_n + A_p)^2}, \tag{37}$$

where we defined

$$c_n - c_p - c_e + c_{\nu_e} = n_{n0}A_n - n_{p0}A_p - n_{e0}A_e + n_{\nu_e0}A_{\nu_e} \equiv C_1, \tag{38}$$

$$c_n - c_p - c_\mu + c_{\nu_\mu} = n_{n0}A_n - n_{p0}A_p - n_{\mu0}A_\mu + n_{\nu_\mu0}A_{\nu_\mu} \equiv C_2. \tag{39}$$

Extracting the real part of Equation (37) and recalling the definition of the bulk viscosity $\text{Re}\Pi = -\zeta\theta$ we find

$$\zeta = \frac{\lambda_e\lambda_\mu \left\{ \lambda_e [(A_n + A_p)C_1 - A_1C_2]^2 + \lambda_\mu [(A_n + A_p)C_2 - A_2C_1]^2 \right\} + \omega^2(\lambda_e C_1^2 + \lambda_\mu C_2^2)}{\left\{ \lambda_e\lambda_\mu [A_1A_2 - (A_n + A_p)^2] - \omega^2 \right\}^2 + \omega^2(\lambda_e A_1 + \lambda_\mu A_2)^2}. \tag{40}$$

If we neglect the muonic contribution then we arrive at

$$\zeta_e = \frac{C_1^2}{A_1} \frac{\gamma_e}{\omega^2 + \gamma_e^2}, \tag{41}$$

with $\gamma_e = \lambda_e A_1$, which coincides with the result of Ref. [18].

In the limit of high frequencies $\omega \gg \lambda_l A_i$ we find from Equation (40)

$$\zeta = \frac{\lambda_e C_1^2 + \lambda_\mu C_2^2}{\omega^2} = \zeta_e + \zeta_\mu, \tag{42}$$

where ζ_e and ζ_μ are the partial bulk viscosities by electronic and muonic Urca processes, respectively [10].

In the opposite limit of low frequencies we find

$$\zeta = \frac{\lambda_e(C_1 - a_1C_2)^2 + \lambda_\mu(C_2 - a_2C_1)^2}{\lambda_e\lambda_\mu(A_n + A_p)^2(a_1a_2 - 1)^2}, \tag{43}$$

with $a_1 = A_1/(A_n + A_p)$ and $a_2 = A_2/(A_n + A_p)$.

4. Numerical Results

The numerical calculations are performed within the framework of covariant density functional approach to the nuclear matter with density-dependent nucleon–meson couplings. The Lagrangian density reads

$$\begin{aligned} \mathcal{L} = & \sum_N \bar{\psi}_N \left[\gamma^\mu \left(i\partial_\mu - g_\omega \omega_\mu - \frac{1}{2} g_\rho \boldsymbol{\tau} \cdot \boldsymbol{\rho}_\mu \right) - m_N^* \right] \psi_N + \sum_\lambda \bar{\psi}_\lambda (i\gamma^\mu \partial_\mu - m_\lambda) \psi_\lambda, \tag{44} \\ & + \frac{1}{2} \partial^\mu \sigma \partial_\mu \sigma - \frac{1}{2} m_\sigma^2 \sigma^2 - \frac{1}{4} \omega^{\mu\nu} \omega_{\mu\nu} + \frac{1}{2} m_\omega^2 \omega^\mu \omega_\mu - \frac{1}{4} \boldsymbol{\rho}^{\mu\nu} \boldsymbol{\rho}_{\mu\nu} + \frac{1}{2} m_\rho^2 \boldsymbol{\rho}^\mu \cdot \boldsymbol{\rho}_\mu, \end{aligned}$$

where N sums over nucleons, ψ_N are the nucleonic Dirac fields, $m_N^* = m_N - g_\sigma \sigma$ are the nucleon effective masses, with m_N being the nucleon mass in vacuum. Next, σ, ω_μ , and $\boldsymbol{\rho}_\mu$ are the scalar-isoscalar, vector-isoscalar, and vector-isovector meson fields, respectively; $\omega_{\mu\nu} = \partial_\mu \omega_\nu - \partial_\nu \omega_\mu$ and $\boldsymbol{\rho}_{\mu\nu} = \partial_\mu \boldsymbol{\rho}_\nu - \partial_\nu \boldsymbol{\rho}_\mu$ are the field strength tensors of vector mesons; m_i are the meson masses and g_i are the baryon-meson couplings with $i = \sigma, \omega, \rho$. Finally, ψ_λ are the leptonic free Dirac fields with masses m_λ . Below we will adopt the DDME2 parametrization of the couplings g_i [21] with the numerical implementation given in Ref. [28].

The composition of beta-equilibrated $npe\mu$ matter in two regimes of low and high temperatures is shown in Figure 1. The proton fraction in the neutrino-transparent matter remains below

the threshold value required for the direct Urca processes to operate in the low-temperature regime in the whole density range considered here ($0.5n_0 \leq n_B \leq 5n_0$). The threshold values of the proton fraction for electronic and muonic Urca processes are $Y_p \approx 13\%$ and $Y_p \approx 16\%$, respectively, whereas the proton fraction remains below 12.5% up to the density $n_B = 5n_0$. Note that in this case at very low densities the net neutrino densities become negative, indicating that the matter contains more antineutrinos than neutrinos in that regime.

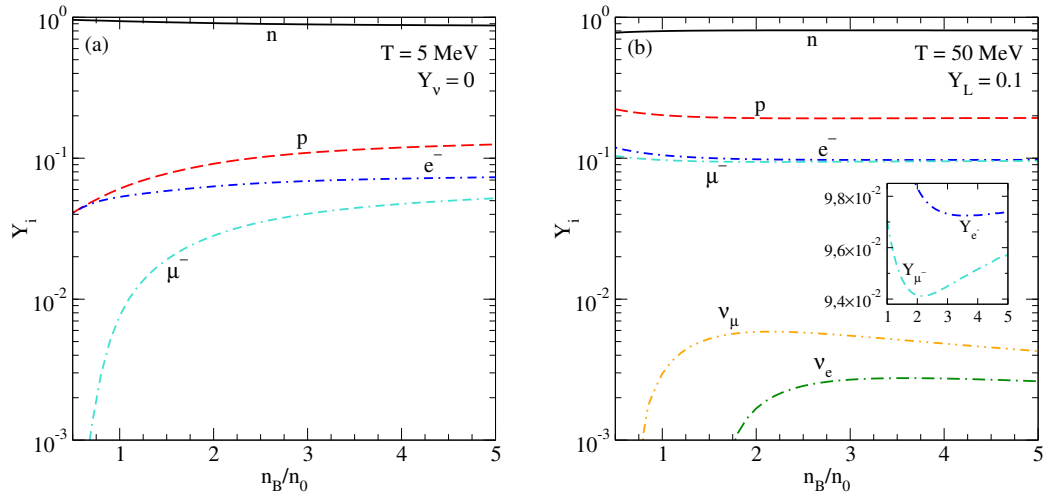


Figure 1. Composition of neutron star merger matter in the DDME2 model, in neutrino-transparent regime with $T = 5$ MeV (a) and neutrino-trapped regime with $T = 50$ MeV (b). The inset shows the minima in the electron and μ -on fractions, at which the subsystems of electrons and muons are scale-invariant, and the corresponding partial bulk viscosities vanish.

4.1. Equilibration Rates of Weak Processes

The electron-producing neutron decay and electron capture rates for neutrino-transparent matter are shown in Figure 2 as functions of the temperature. The equilibration rates rapidly increase with increasing temperature as a result of the fast opening of the scattering phase space. We see also that the neutron decay rate is suppressed as compared to the electron capture rate at least by three orders of magnitude, and is exponentially damped at low temperatures and high densities because of diminished scattering phase space (there are no curves corresponding to $n_B = 3n_0$ and $n_B = 5n_0$ in panel (a) as the rate is highly damped in these cases). Similar behavior for the neutron decay rate was found also for other EoS models in Ref. [29]. As a result, under the condition $\mu_n = \mu_p + \mu_e$ the neutron decay and electron capture rates do not balance each other, which implies that the matter is out of β -equilibrium. As noted in the discussion of Equations (15) and (16), in principle this shows the need for a nonzero isospin chemical potential. However, as the main focus of this work is to study how the muonic reactions contribute to the bulk viscosity of $npe\mu$ matter, below we will neglect that finite temperature correction, given that it would not change the value of bulk viscosity at the maximum, and (because the rates are so sensitive to temperature) would only shift the temperature at which that maximum is attained by about 1 MeV.

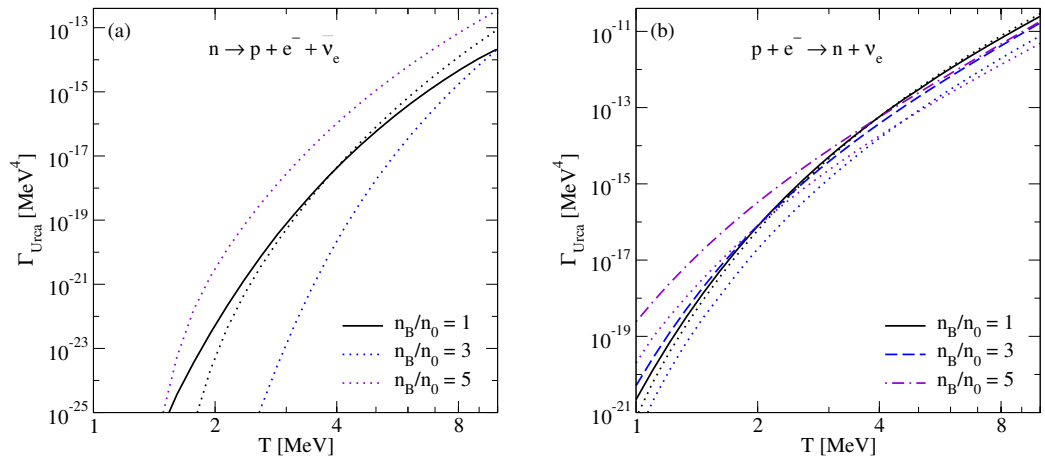


Figure 2. The rates of neutron e -decay (a) and electron capture (b) processes as functions of the temperature for various densities for neutrino-transparent matter. The dotted lines show the rates of the same processes computed in Ref. [18] within the approximation of nonrelativistic nucleons.

We show also the electron-capture rates in Figure 2 which were computed in Ref. [18] in the approximation of nonrelativistic nucleons by dotted lines. We see that the nonrelativistic approximation underestimates the exact electron capture rates by up to an order of magnitude (at $n_B = 5n_0$). This is not the case for the neutron decay process which shows finite nonrelativistic rates also at high densities where the exact relativistic calculations predict their strong suppression by an exponential (Boltzmann-type) factor.

Panel (a) of Figure 3 shows the muon capture rates, the general behavior of which is similar to the electron capture rates. Quantitatively, the muon capture rate is much smaller at low temperatures and becomes comparable to the electron capture rate above $T \geq 5$ MeV. The rate of the neutron μ -decay is always smaller than those of other processes that affect muon density by at least three orders of magnitude over the density and temperature range considered here and is not shown.

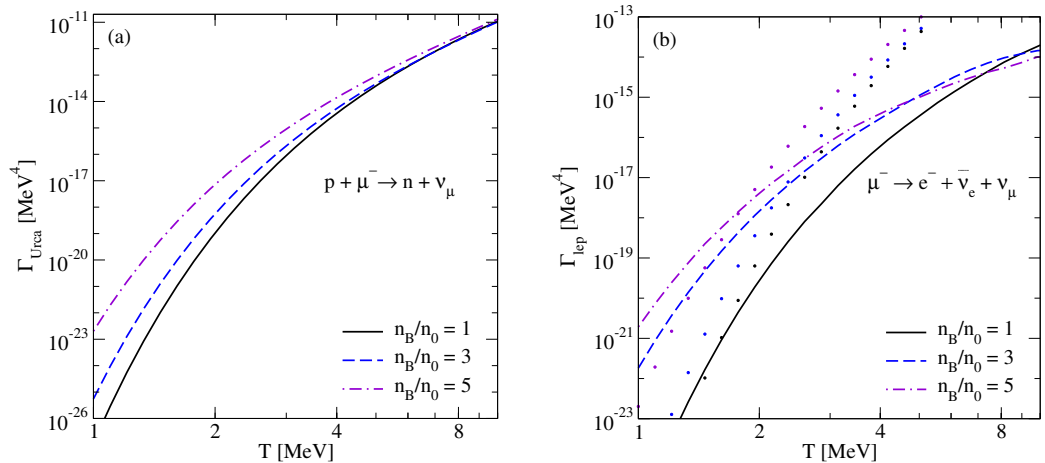


Figure 3. The rates of muon capture (a) and muon decay (b) processes as functions of the temperature for various densities for neutrino-transparent matter. The neutron μ -decay rate is strongly damped as compared to the muon capture rate. The dotted lines in panel (b) show the muon capture rates.

Panel (b) of Figure 3 shows the rate of the muon decay (3). The muon decay process has the same kinematics as the neutron decay. As a result, the temperature dependence of the

muon decay rate is qualitatively very similar to that of neutron decay if it is finite. To compare the Urca and leptonic reaction rates we show in Figure 3b the muon capture rates by dotted lines (electron capture rates are much larger than the muon decay rates and are not shown here). We see, that, typically, the Urca reaction rates are much larger than the leptonic reaction rates, the only exception being the range of very low temperatures $T \lesssim 2$ MeV, where both processes involving muons are much slower than electron capture process. In this narrow range of temperatures, the muonic contribution to the bulk viscosity can be neglected, whereas at higher temperatures both electronic and muonic Urca processes should be accounted for with leptonic reactions assumed to be frozen, as discussed in Section 3.

Figure 4 shows the rates of the electron (a) and muon (b) capture processes in the neutrino-trapped regime. At moderate temperatures $T \leq 10$ MeV, the lepton capture rates follow their low-temperature scaling $\propto T^3$ [20]. The electron and muon capture rates are very similar both qualitatively and quantitatively. Panel (a) shows also the electron-capture rates of nuclear matter in the approximation of nonrelativistic nucleons [18]. As in the neutrino-transparent case, the non-relativistic approximation underestimates the exact equilibration rates also in the neutrino-trapped regime by a factor that rises with the density from 1 to 10. As for the neutron decay processes (1), their rates are many orders of magnitude smaller than the lepton capture rates as the formers involve antineutrinos instead of neutrinos. A detailed discussion on the relative importance of the neutron decay and lepton capture rates can be found in Ref. [20].

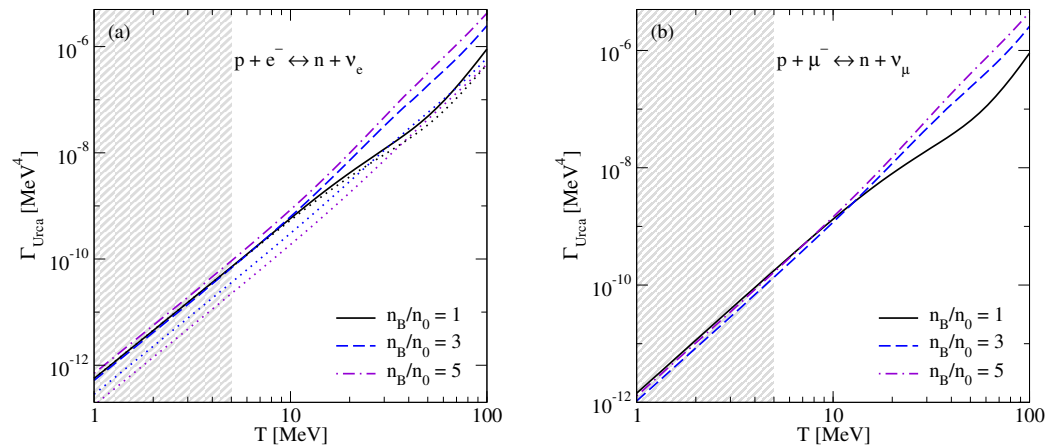


Figure 4. The electron (a) and muon (b) capture rates as functions of the temperature for various densities for the neutrino-trapped matter. The neutron decay rates are negligible compared to the lepton capture rates in the whole temperature-density range. The shaded areas show the neutrino transparent region of temperatures $T \leq 5$ MeV. The dotted lines in panel (a) show the nonrelativistic approximation to the electron capture rates as computed in Ref. [18].

Figure 5 shows the rates of neutrino (a) and antineutrino (b) absorption processes. The neutrino absorption rates show similar to the lepton capture rates behavior (shown by dotted lines) but are smaller on average by an order of magnitude. As expected, the antineutrino absorption rates are much smaller than the neutrino absorption rates. The muon decay rate is even smaller than the antineutrino absorption process because of the very small scattering phase space. Thus, we conclude that the leptonic processes are always much slower than the Urca processes also in the neutrino-trapped matter.

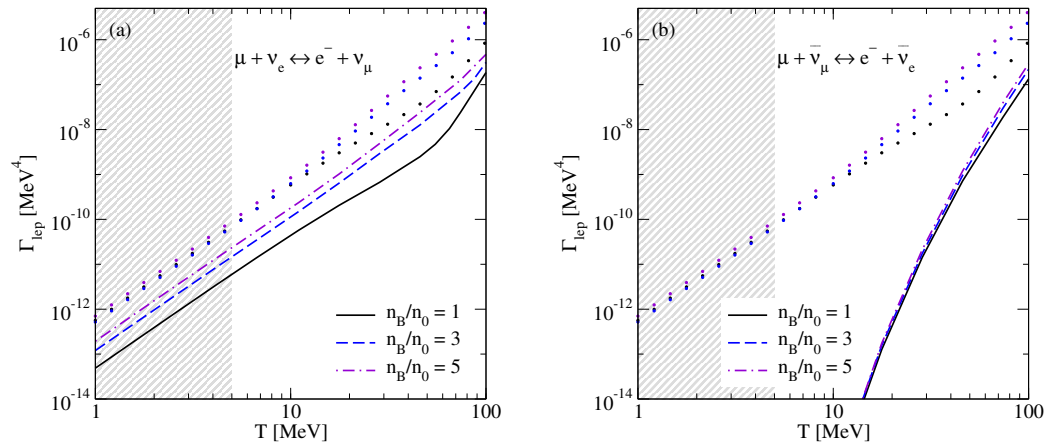


Figure 5. Rates of the neutrino (a) and antineutrino (b) absorption processes as functions of the temperature for different values of the density for the neutrino-trapped matter. The electron (Urca) capture rates are shown by dotted lines for comparison; the muon capture rates are slightly higher than the electron capture rates and are not shown. The shaded areas show the neutrino transparent region of temperatures $T \leq 5$ MeV.

4.2. Susceptibilities and Urca Relaxation Rates

We have extended our work on the bulk viscosities in the isothermal regime to the case of isentropic matter. Here among other things we compare the isothermal and isentropic results leaving the detailed discussion of the latter to a future work [30].

Figure 6 shows the susceptibilities C_1^2/A_1 and C_2^2/A_2 (as computed in Ref. [20]) which enter the formulas of the partial bulk viscosities from electronic (ζ_e) and muonic (ζ_μ) Urca processes (note that ζ_μ should be obtained from Equation (41) by replacing $A_1 \rightarrow A_2, C_1 \rightarrow C_2$ and $\gamma_e \rightarrow \gamma_\mu = \lambda_\mu A_2$). Panels (a) and (b) show the results for neutrino-transparent and neutrino-trapped matter, respectively. The solid curves correspond to isothermal, and the dashed lines—to adiabatic susceptibilities. In the neutrino-transparent regime, the susceptibilities are sensitive to the density and temperature only in the low-density region, where the difference between isothermal and adiabatic susceptibilities is the largest (e.g., the ratio of adiabatic and isothermal C_1^2/A_1 is around 1.67 at $n_B = 0.5n_0$ and $T = 5$ MeV). In the high-temperature regime of neutrino-trapped matter, there are special values of the density where C_1^2/A_1 and C_2^2/A_2 , and therefore, also the partial bulk viscosities ζ_e and ζ_μ drop to zero as a result of the subsystems of electrons and muons, respectively becoming scale-invariant at those points. At those points the electron and muon fractions become independent of the baryon density, as seen from the inset of Figure 1 (the small shift of the special point in the electron susceptibility from the minimum of the electron fraction is a result of the approximations made in the evaluation of the susceptibilities).

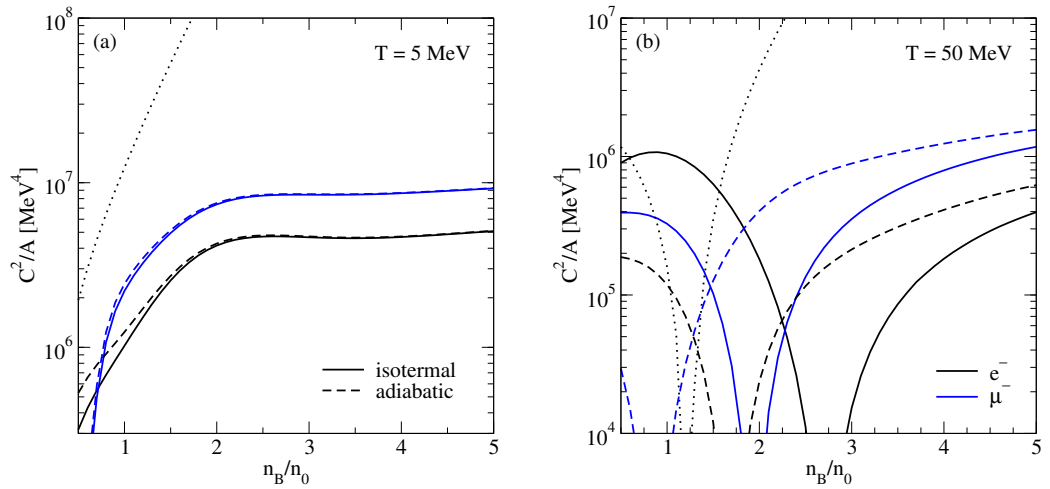


Figure 6. The susceptibilities C_1^2/A_1 and C_2^2/A_2 corresponding to electronic and muonic bulk viscosities as functions of the baryon density for neutrino-transparent matter (a) and neutrino-trapped matter (b). The solid lines show isothermal susceptibilities, and the dashed lines show the adiabatic susceptibilities. The dotted lines show the nonrelativistic approximation to the isothermal C_1^2/A_1 [18].

In contrast to the low-temperature regime, the difference between isothermal and adiabatic susceptibilities is significant in the neutrino-trapped matter. Typically, the adiabaticity shifts the scale-invariant points to lower densities by about one nuclear density as compared to the isothermal case. The muonic and electronic susceptibilities differ on average by factors from 2 to 5 in both regimes (except the domain of very low densities below the muon threshold in the neutrino-transparent matter, and the vicinity of the scale-invariant point in the case of neutrino-trapped matter). Next, comparing the panels (a) and (b) of Figure 6, we see that the susceptibilities are roughly an order of magnitude larger in the neutrino-transparent regime. We see also that the nonrelativistic approximation to nucleons strongly overestimates the susceptibilities.

The relaxation rates $\gamma_e = \lambda_e A_1$ and $\gamma_\mu = \lambda_\mu A_2$ of electronic and muonic Urca processes, respectively, are shown in Figure 7. In the neutrino-transparent regime, γ_e and γ_μ cross the curves of the constant frequencies $f \equiv \omega/2\pi = 1$ kHz and $f \equiv \omega/2\pi = 10$ kHz (1 kHz corresponds to $4.14 \cdot 10^{-18}$ MeV) at temperatures in the range $3 \leq T \leq 8$ MeV. Around these temperatures, the bulk viscosity of $npe\mu$ matter shows a resonant maximum. In the neutrino-trapped regime, the relaxation rates are always higher than the typical oscillation frequencies, and the bulk viscosity is independent of the oscillation frequency.

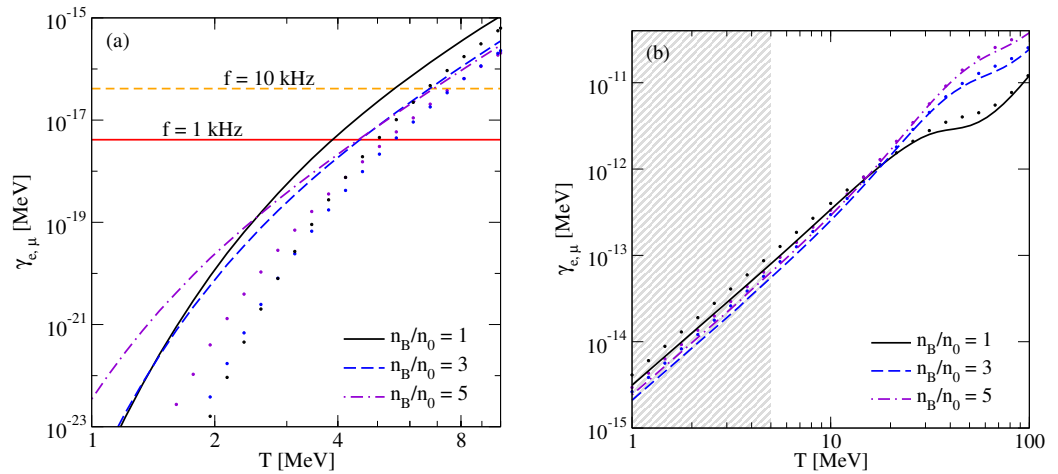


Figure 7. The relaxation rates γ_e (solid, dashed, and dash-dotted lines) and γ_μ (dotted lines) of Urca processes as functions of the temperature for fixed values of the density for (a) neutrino-transparent matter; (b) neutrino-trapped matter, where the shaded area shows the extrapolation of the result to the temperature regime $T \leq 5$ MeV, where the trapping assumption fails. The horizontal lines in panel (a) correspond to the fixed values of oscillation frequency $f = 1$ kHz (solid line) and $f = 10$ kHz (dashed line).

4.3. Bulk Viscosity of $npe\mu$ Matter in the Isothermal Case

The results for the bulk viscosity of relativistic $npe\mu$ matter (computed with the isothermal susceptibilities) are shown in Figure 8. Panel (a) shows the results for neutrino-transparent matter at frequency $f = 1$ kHz, which is typical for density oscillations in neutron star mergers. At low temperatures, where $\lambda_l A_j \ll \omega$, the bulk viscosity is given by the sum of electronic and muonic partial viscosities, $\zeta = \zeta_e + \zeta_\mu \propto \omega^{-2}$, see Equation (42). In this regime we have typically $\zeta_\mu \ll \zeta_e$, and the bulk viscosity of $npe\mu$ matter practically coincides with that of npe matter which is shown in Figure 8 by dotted lines. For the given frequency the bulk viscosity of $npe\mu$ matter has a resonant maximum at a temperature between the resonant temperatures T_l of partial bulk viscosities ζ_l , where $\omega = \gamma_l(T_l)$ with $l = \{e, \mu\}$. The maximum of the bulk viscosity of $npe\mu$ matter is located at a slightly higher temperature as compared to the bulk viscosity of npe matter. At temperatures above the maximum, where $\lambda_l A_j \gg \omega$, the bulk viscosity becomes frequency-independent. In this regime, the bulk viscosity of $npe\mu$ matter exceeds the bulk viscosity of npe matter by factors between 2.5 and 8.

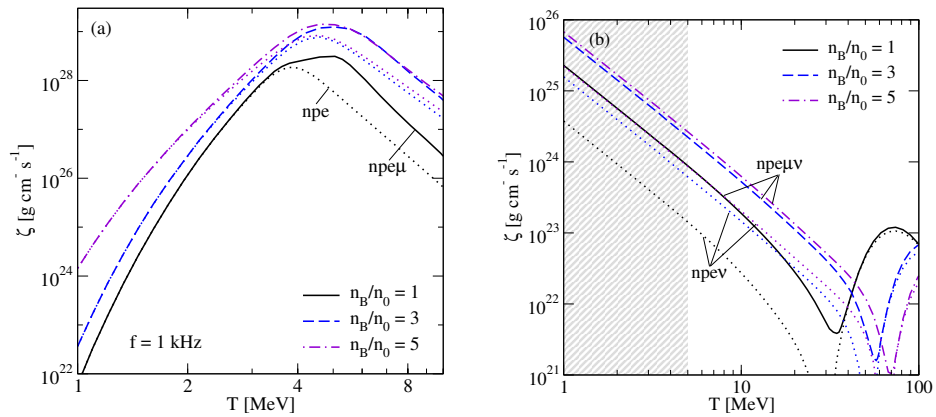


Figure 8. The bulk viscosity of relativistic $npe\mu$ matter as a function of the temperature for (a) neutrino-transparent matter at $f = 1$ kHz; (b) neutrino-trapped matter. The region $T \leq 5$ MeV in panel (b) is shaded because neutrinos are no longer trapped at those temperatures. The dotted lines show the bulk viscosities of relativistic npe matter.

As in the neutrino-trapped matter, the equilibration rates are much larger than the oscillation frequency, the bulk viscosity is given by the frequency-independent Formula (43). In the high-temperature range we have mainly $(A_n + A_p)C_1 \ll A_1C_2$, $(A_n + A_p)C_2 \ll A_2C_1$, $(A_n + A_p)^2 \ll A_1A_2$, which allows to simplify Equation (43) to

$$\zeta \simeq \frac{\lambda_e(A_1C_2)^2 + \lambda_\mu(A_2C_1)^2}{\lambda_e\lambda_\mu(A_1A_2)^2} = \frac{C_1^2}{A_1} \frac{1}{\gamma_e} + \frac{C_2^2}{A_2} \frac{1}{\gamma_\mu} = \zeta_e + \zeta_\mu. \tag{45}$$

As the susceptibilities, C_1 and C_2 cross zero at high temperatures, the partial bulk viscosities drop to zero at those points as well. The summed ζ will thus obtain a minimum at an intermediate temperature but will remain finite at the minimum. The generic behavior of the bulk viscosity of $npe\mu$ matter is similar to the one of npe matter. The former exceeds the latter by factors from 3 to 10 on the left side of the minimum, whereas to the right side of the minimum the muonic contribution to the bulk viscosity is negligible.

We also note that the nonrelativistic approximation would highly overestimate the bulk viscosities in the whole temperature-density regime considered because this approximation leads to an underestimate of the equilibration rates and an overestimate of the susceptibilities.

4.4. Damping of Density Oscillations

Now we estimate the bulk viscous damping timescales of density oscillations in relativistic $npe\mu$ matter. The damping timescale is given by [17,31,32]

$$\tau_\zeta = \frac{1}{9} \frac{Kn_B}{\omega^2 \zeta}, \tag{46}$$

where ϵ is the energy density of the system, and

$$K = 9n_B \frac{\partial^2 \epsilon}{\partial n_B^2} \tag{47}$$

is the incompressibility of nuclear matter. It depends weakly on the temperature in both regimes of neutrino-transparent and neutrino-trapped matter [18], therefore the temperature dependence of the damping timescale is practically the inverse temperature dependence of the bulk viscosity. Figure 9 shows the damping timescale for two oscillation frequencies: panel (a)

with $f = 1$ kHz, and panel (b) with $f = 10$ kHz. In each of the panels, we combined the results of neutrino-transparent ($1 \leq T \leq 5$ MeV) and neutrino-trapped matter ($10 \leq T \leq 100$ MeV). For intermediate temperatures $5 \leq T \leq 10$ MeV the results are extrapolated between these two regimes with dashed lines. The damping timescale attains its minimum around $T = 5$ MeV, with its value being inversely proportional to the frequency. In the low-temperature regime (to the left side of the minimum) the damping timescale is frequency-independent but becomes inversely proportional to the square of ω in the neutrino-trapped regime as the bulk viscosity is independent of the oscillation frequency there.

The shaded areas in Figure 9 separate the temperature-density range where the damping timescale becomes smaller than the early (≈ 10 ms, dark shaded areas) and long-term (≈ 1 s, lightly shaded areas) evolution timescales of post-merger object, respectively. For a typical frequency $f = 1$ kHz, the bulk viscous damping is efficient in short-living remnants only at low densities $n_B \leq n_0$ in the temperature range $4 \leq T \leq 6$ MeV. At higher densities, the damping could be relevant during the long-term evolution only. For higher frequencies, there is a larger domain of densities and temperatures where the damping timescales reach down to the short-term evolution timescale of BNS mergers. For example, for $f = 10$ kHz the short-term damping is efficient at densities $n_B \leq 2n_0$ and for temperatures between $3 \leq T \leq 7$ MeV. The dynamics of long-living remnants would be affected by the bulk viscosity for a wider temperature-density range, typically $2 \leq T \leq 10$ MeV and $n_B \leq 5n_0$.

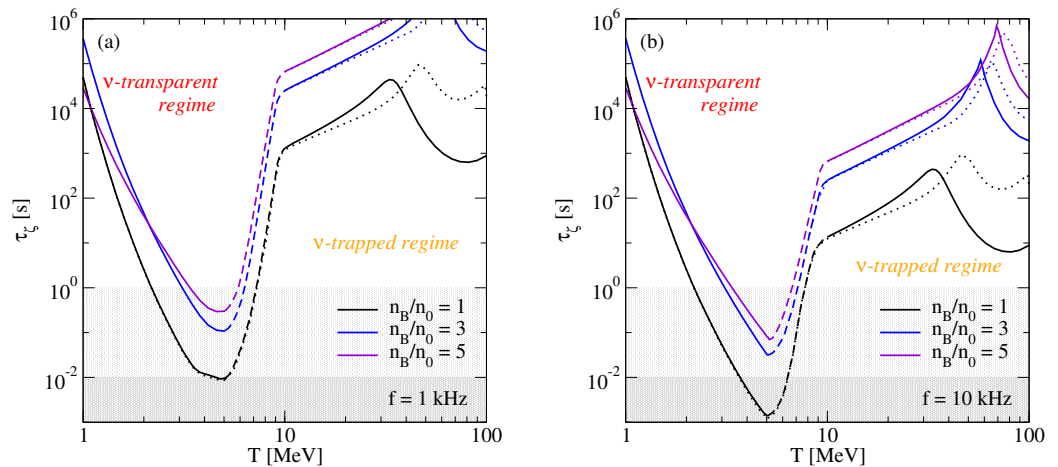


Figure 9. The oscillation damping timescale as a function of temperature for various densities for frequency fixed at (a) $f = 1$ kHz; (b) $f = 10$ kHz. The solid lines show the results obtained with isothermal, and the dotted lines—with adiabatic susceptibilities. The dashed lines interpolate between the results of neutrino-transparent and neutrino-trapped regimes.

For the sake of completeness, we show also the damping timescales computed with adiabatic susceptibilities with dotted lines in Figure 9. Note that the bulk viscosities and the damping timescales calculated in Ref. [17] used the adiabatic susceptibilities and compressibilities. It was found that the bulk viscosities and the damping timescales for adiabatic and isothermal oscillations in the neutrino-transparent matter differ by a factor of around 2 in the regime where the bulk viscous damping is efficient in the post-merger dynamics. This is fully consistent with our findings, see Figure 9. As expected, the adiabaticity modifies the results significantly only in the high-temperature regime, where it can increase τ_ζ by more than an order of magnitude. However, in the high-temperature regime of neutrino-trapped matter the Urca-process-driven bulk viscosity is not sufficiently large to affect the evolution of BNS mergers.

5. Conclusions

In this work, we provided a brief review of our work on the Urca-process-driven bulk viscosity of relativistic $npe\mu$ matter in the parameter range relevant to binary neutron star mergers. We focused on the semi-leptonic Urca processes as well as leptonic processes in $npe\mu$ matter in two different regimes of interest: (a) neutrino-transparent regime where $T \leq T_{\text{tr}}$ with $T_{\text{tr}} \simeq 5 \div 10$ MeV being the neutrino-trapping temperature; and (b) neutrino-trapped regime at $T \geq T_{\text{tr}}$. Along with the results for the bulk viscosity in the neutrino-trapped regime obtained earlier in Ref. [20], we showed novel results for the neutrino-transparent matter as well as some results pertaining to the case of isentropic instead of isothermal oscillations.

Our main observations can be summarized as follows:

- (a) We observe that the leptonic reactions proceed much slower than the Urca process in the entire temperature-density range. In the neutrino-transparent matter the dominant leptonic reaction is the muon decay, whereas in the neutrino-trapped regime, the dominant leptonic reactions are the neutrino and antineutrino absorption processes.
- (b) As a result, the bulk viscosity of $npe\mu$ matter can be computed assuming that the leptonic processes are frozen. Qualitatively, the bulk viscosity of $npe\mu$ matter exceeds that of npe matter by factors from 2.5 to 8 above the maximum temperature in the ν -transparent matter, and by factors from 1 to 10 in the ν -trapped matter.
- (c) The bulk viscosity features its resonant maximum at a temperature where the average β -relaxation rate of electronic and muonic Urca processes coincides with the angular frequency of density oscillations. This resonant maximum appears around $T \simeq 5$ MeV where the matter is still transparent to neutrinos. At higher temperatures, bulk viscosity drops rapidly once the matter enters the neutrino-trapped regime. There appear sharp minima in the bulk viscosity at $T \geq 30$ MeV where the lepton fractions become independent of the density.
- (d) Using our results for the bulk viscosity we estimate the bulk viscous damping timescales of density oscillations in neutron star mergers. We find that for typical oscillation frequencies $1 \leq f \leq 10$ kHz there is a finite temperature-density range where the bulk viscous dissipation can affect the short-term evolution ($\simeq 10$ ms) of BNS mergers significantly. The damping timescale features a minimum at $T \simeq 5$ MeV with minimum values of the order of ms at very low densities $n_B \leq n_0$. At higher densities, the damping timescales of density oscillations are larger and can affect the post-merger evolution only on a long-time scale. At high temperatures where neutrinos are trapped in the matter, the damping timescales are much longer; therefore, the Urca processes are not the dominant channels by which to damp the density oscillations in BNS mergers.

Author Contributions: The authors contributed equally to this research. All authors have read and agreed to the published version of the manuscript.

Funding: The research of M.A. was funded by the U.S. Department of Energy, Office of Science, Office of Nuclear Physics under Award Number No. DE-FG02-05ER41375. The research of A.H. and A.S. was funded by the Volkswagen Foundation (Hannover, Germany) grant No. 96 839 and the European COST Action “PHAROS” (CA16214). The research of A.S. was funded by Deutsche Forschungsgemeinschaft Grant No. SE 1836/5-2 and the Polish NCN Grant No. 2020/37/B/ST9/01937 at Wroclaw University.

Data Availability Statement: Not applicable.

Conflicts of Interest: The authors declare no conflict of interest.

References

1. Endrizzi, A.; Logoteta, D.; Giacomazzo, B.; Bombaci, I.; Kastaun, W.; Ciolfi, R. Effects of chiral effective field theory equation of state on binary neutron star mergers. *Phys. Rev. D* **2018**, *98*, 043015. [[CrossRef](#)]

2. Most, E.R.; Papenfort, L.J.; Rezzolla, L. Beyond second-order convergence in simulations of magnetized binary neutron stars with realistic microphysics. *MNRAS* **2019**, *490*, 3588–3600. [[CrossRef](#)]
3. Ciolfi, R.; Kastaun, W.; Kalinani, J.V.; Giacomazzo, B. First 100 ms of a long-lived magnetized neutron star formed in a binary neutron star merger. *Phys. Rev. D* **2019**, *100*, 023005. [[CrossRef](#)]
4. Tsokaros, A.; Ruiz, M.; Paschalidis, V.; Shapiro, S.L.; Uryū, K. Effect of spin on the inspiral of binary neutron stars. *Phys. Rev. D* **2019**, *100*, 024061. [[CrossRef](#)]
5. Most, E.R.; Haber, A.; Harris, S.P.; Zhang, Z.; Alford, M.G.; Noronha, J. Emergence of microphysical viscosity in binary neutron star post-merger dynamics. *arXiv* **2022**, arXiv:2207.00442.
6. Sawyer, R.F.; Soni, A. Transport of neutrinos in hot neutron-star matter. *ApJ* **1979**, *230*, 859–869. [[CrossRef](#)]
7. Sawyer, R.F. Damping of neutron star pulsations by weak interaction processes. *ApJ* **1980**, *237*, 187–197. [[CrossRef](#)]
8. Sawyer, R.F. Bulk viscosity of hot neutron-star matter and the maximum rotation rates of neutron stars. *Phys. Rev. D* **1989**, *39*, 3804–3806. [[CrossRef](#)]
9. Haensel, P.; Schaeffer, R. Bulk viscosity of hot-neutron-star matter from direct URCA processes. *Phys. Rev. D* **1992**, *45*, 4708–4712. [[CrossRef](#)]
10. Haensel, P.; Levenfish, K.P.; Yakovlev, D.G. Bulk viscosity in superfluid neutron star cores. I. Direct Urca processes in $n\mu$ matter. *A&A* **2000**, *357*, 1157–1169.
11. Haensel, P.; Levenfish, K.P.; Yakovlev, D.G. Bulk viscosity in superfluid neutron star cores. II. Modified Urca processes in $n\mu$ matter. *A&A* **2001**, *372*, 130–137. [[CrossRef](#)]
12. Haensel, P.; Levenfish, K.; Yakovlev, D. Bulk viscosity in superfluid neutron star cores. III. Effects of sigma-hyperons. *A&A* **2002**, *381*, 1080–1089. [[CrossRef](#)]
13. Dong, H.; Su, N.; Wang, Q. Bulk viscosity in nuclear and quark matter. *J. Phys. Nucl. Phys.* **2007**, *34*, S643–S646. [[CrossRef](#)]
14. Alford, M.G.; Mahmoodifar, S.; Schwenzer, K. Large amplitude behavior of the bulk viscosity of dense matter. *J. Phys. Nucl. Phys.* **2010**, *37*, 125202. [[CrossRef](#)]
15. Alford, M.G.; Good, G. Leptonic contribution to the bulk viscosity of nuclear matter. *Phys. Rev.* **2010**, *C82*, 055805. [[CrossRef](#)]
16. Kolomeitsev, E.E.; Voskresensky, D.N. Viscosity of neutron star matter and r-modes in rotating pulsars. *Phys. Rev. C* **2015**, *91*, 025805. [[CrossRef](#)]
17. Alford, M.G.; Harris, S.P. Damping of density oscillations in neutrino-transparent nuclear matter. *Phys. Rev. C* **2019**, *100*, 035803. [[CrossRef](#)]
18. Alford, M.; Harutyunyan, A.; Sedrakian, A. Bulk viscosity of baryonic matter with trapped neutrinos. *Phys. Rev. D* **2019**, *100*, 103021. [[CrossRef](#)]
19. Alford, M.G.; Haber, A. Strangeness-changing rates and hyperonic bulk viscosity in neutron star mergers. *Phys. Rev. C* **2021**, *103*, 045810. [[CrossRef](#)]
20. Alford, M.; Harutyunyan, A.; Sedrakian, A. Bulk viscosity from Urca processes: $n\mu$ matter in the neutrino-trapped regime. *Phys. Rev. D* **2021**, *104*, 103027. [[CrossRef](#)]
21. Lalazissis, G.A.; Nikšić, T.; Vretenar, D.; Ring, P. New relativistic mean-field interaction with density-dependent meson-nucleon couplings. *Phys. Rev. C* **2005**, *71*, 024312. [[CrossRef](#)]
22. Reed, B.T.; Fattoyev, F.J.; Horowitz, C.J.; Piekarewicz, J. Implications of PREX-2 on the Equation of State of Neutron-Rich Matter. *Phys. Rev. Lett.* **2021**, *126*, 172503. [[CrossRef](#)] [[PubMed](#)]
23. Reinhard, P.-G.; Roca-Maza, X.; Nazarewicz, W. Information Content of the Parity-Violating Asymmetry in ^{208}Pb . *Phys. Rev. Lett.* **2021**, *127*, 232501.
24. Alford, M.G.; Harris, S.P. β equilibrium in neutron-star mergers. *Phys. Rev. C* **2018**, *98*, 065806. [[CrossRef](#)]
25. Baiotti, L. Gravitational waves from neutron star mergers and their relation to the nuclear equation of state. *Prog. Part. Nucl. Phys.* **2019**, *109*, 103714. [[CrossRef](#)]
26. Greiner, W.; Müller, B. *Gauge Theory of Weak Interactions*; Physics and Astronomy Online Library; Springer: Berlin/Heidelberg, Germany, 2000.
27. Guo, G.; Martínez-Pinedo, G.; Lohs, A.; Fischer, T. Charged-Current Muonic Reactions in Core-Collapse Supernovae. *Phys. Rev. D* **2020**, *102*, 023037. [[CrossRef](#)]
28. Colucci, G.; Sedrakian, A. Equation of state of hypernuclear matter: Impact of hyperon-scalar- meson couplings. *Phys. Rev. C* **2013**, *87*, 055806. [[CrossRef](#)]
29. Alford, M.G.; Haber, A.; Harris, S.P.; Zhang, Z. Beta Equilibrium Under Neutron Star Merger Conditions. *Universe* **2021**, *7*, 399. [[CrossRef](#)]
30. Alford, M.; Harutyunyan, A.; Sedrakian, A. Bulk viscosity from Urca processes: $n\mu$ matter in the neutrino-transparent regime. 2022, *preprint*.
31. Alford, M.G.; Bovard, L.; Hanauske, M.; Rezzolla, L.; Schwenzer, K. Viscous Dissipation and Heat Conduction in Binary Neutron-Star Mergers. *Phys. Rev. Lett.* **2018**, *120*, 041101. [[CrossRef](#)]

-
32. Alford, M.; Harutyunyan, A.; Sedrakian, A. Bulk Viscous Damping of Density Oscillations in Neutron Star Mergers. *Particles* **2020**, *3*, 500–517. [[CrossRef](#)]